

Orthorhombic distortion drives orbital ordering in the antiferromagnetic $3d^1$ Mott insulator PrTiO_3

Prithwjit Mandal^{1,*}, Shashank Kumar Ojha¹, Duo Wang^{2,3}, Ranjan Kumar Patel¹, Siddharth Kumar¹,
 Jyotirmay Maity¹, Zhan Zhang⁴, Hua Zhou⁴, Christoph Klewe⁵, Padraic Shafer⁵,
 Biplab Sanyal^{2,†} and Srimanta Middey^{1,‡}

¹*Department of Physics, Indian Institute of Science, Bengaluru 560012, India*

²*Department of Physics and Astronomy, Uppsala University, Uppsala 75120, Sweden*

³*Faculty of Applied Sciences, Macao Polytechnic University, Macao SAR 999078, China*

⁴*Advanced Photon Source, Argonne National Laboratory, Lemont, Illinois 60439, USA*

⁵*Advanced Light Source, Lawrence Berkeley National Laboratory, Berkeley, California 94720, USA*



(Received 30 September 2022; revised 28 May 2023; accepted 17 July 2023; published 28 July 2023)

The orbital, which represents the shape of the electron cloud, very often strongly influences the manifestation of various exotic phenomena, e.g., magnetism, metal-insulator transition, colossal magnetoresistance, unconventional superconductivity, etc. in solid-state systems. The observation of the antiferromagnetism in $RE\text{TiO}_3$ (RE = rare-earth) series has been puzzling since the celebrated Kugel-Khomskii model of spin-orbital superexchange predicts ferromagnetism in an orbitally degenerate d^1 system. Further, the existence of the orbitally ordered vs. orbital liquid phase in both antiferromagnetic and paramagnetic phase have been unsettled issues thus far. To address these longstanding questions, we investigate single crystalline film of PrTiO_3 . Our synchrotron x-ray diffraction measurements confirm the retention of bulklike orthorhombic (D_{2h}) symmetry in the thin film geometry. We observe similar x-ray linear dichroism signal in both paramagnetic and antiferromagnetic phase, which can be accounted by ferro-orbital ordering (FOO). While the presence of D_{2h} crystal field does not guarantee lifting of orbital degeneracy always, we find it to be strong enough in these rare-earth titanates, leading to the FOO state. Thus, our work demonstrates the orthorhombic distortion is the driving force for the orbital ordering of antiferromagnetic $RE\text{TiO}_3$.

DOI: [10.1103/PhysRevB.108.045145](https://doi.org/10.1103/PhysRevB.108.045145)

I. INTRODUCTION

The shape of the quantum mechanical wave function for an electron bound to an atomic nucleus by Coulomb force is determined by the orbital (l) and magnetic quantum (m_l) numbers. When different atoms/ions are combined to form a solid, the azimuthal degeneracy is lifted due to the presence of Coulomb interaction with the neighboring atoms/ions. For example, in transition-metal oxides (TMOs) with octahedral crystal field (CF), the original fivefold degenerate d orbitals [$l = 2; m_l = 0, \pm 1, \pm 2$] of the TM site are split into threefold degenerate t_{2g} orbitals with lower energy and doubly degenerate e_g orbitals with higher energy [1]. Very often, such degeneracy is further lifted by structural distortion, leading to an orbital ordering (OO) [2]. Interestingly, OO can also happen in absence of any CF splitting due to electronic superexchange, popularly known as Kugel-Khomskii mechanism [3]. In reality, both of these mechanisms of OO can coexist and separating the role of electron-lattice vs. spin-orbital coupling is nontrivial due to their comparable energy scale [4]. The presence of OO and its role in magnetism, metal-insulator transition, superconductivity, charge

density wave phase, structural symmetry change, etc. has been demonstrated in various complex oxides (see Refs. [2,5,6] for review).

Rare-earth titanates ($RE\text{TiO}_3$) are considered to be textbook examples of a Mott insulator [7], which are also potential platforms for Mottronics [8] and Floquet orbital engineering [9,10]. They exhibit an interesting phase diagram with a crossover from antiferromagnetic to ferromagnetic phase as a function of Ti-O-Ti bond angle [11]. The origin of ferromagnetic ordering in highly distorted members like YTiO_3 is well understood considering Kugel-Khomskii coupling between spin and orbital degrees of freedom with twofold degenerate lower t_{2g} levels [3,12,13]. On the contrary, the appearance of G -type antiferromagnetic phase for the less distorted members (bulk), e.g., LaTiO_3 (LTO) remains a subject of intense scrutiny without reaching any consensus [13–20]. Antiferromagnetic LTO has only a small distortion of its TiO_6 octahedra [21] and hence the t_{2g} levels were initially considered to be degenerate. This degeneracy would result in ferromagnetism in d^1 system according to the Kugel-Khomskii model [3].

The observation of a small moment on Ti for LTO was thought to be an outcome of sizable spin-orbit coupling [22]. However, such scenario was discarded by the observation of an isotropic spin wave spectra [23]. Also, resonant x-ray scattering study could not reveal any sizable order parameter for orbital ordering [23]. These results were explained by a quantum fluctuation-driven orbital liquid (OL) model [15].

*prithwjitm@iisc.ac.in

†biplab.sanyal@physics.uu.se

‡smiddey@iisc.ac.in

Contrary to this, the presence of rigid ferro-orbital ordering (FOO) was proposed considering the degeneracy lifting of t_{2g} states due to the antiparallel displacement of RE ions [17]. Such a scenario was further promoted by a dynamical mean-field theory (DMFT) study [18]. Several experimental observations have been explained in terms of such a FOO phase [24–26]. Thus, the puzzle about the actual orbital scenario of antiferromagnetic $RETiO_3$ is yet to be solved.

Here, we have explored the multiorbital physics of antiferromagnetic $RETiO_3$ by x-ray linear dichroism spectroscopy (XLD) [27]. We find that the isotropic x-ray absorption spectroscopy fails to differentiate among different symmetries of the crystal field for $RETiO_3$, and XLD experiments play a pivotal role to settle the debate between FOO and OL state. Our results clarify that the level splitting due to D_{2h} symmetry is strong enough to favor OO, which is further corroborated by density functional theory. We also find the OO pattern is independent of the magnetic transition, resolving another unsettled issue about the role of antiferromagnetism in setting OO in $RETiO_3$ [26,28,29].

II. METHODS

A. Growth and characterization

To examine orbital physics, we have investigated thin epitaxial $PrTiO_3$ (PTO) films [thickness: 10–20 uc] grown on $NdGaO_3$ (NGO) $(110)_{or} \equiv (001)_{pc}$ substrates by pulsed laser deposition (or, pc denotes orthorhombic, pseudocubic setting, also see Sec. S1 of SM [30]). A comprehensive sample characterization using reflection high-energy electron diffraction, atomic force microscopy, x-ray reflectivity and x-ray diffraction have confirmed the single crystalline perovskite phase of the films with smooth surface morphology (Sec. S2 of SM [30]). We have carefully chosen this compound as the bulk PTO has a lower Ti-O-Ti bond angle compared to LTO, which would enhance the $GdFeO_3$ distortion. Also, the higher Mott gap makes PTO a robust insulator, unlike LTO, which easily becomes metallic by excess oxygen doping [8]. The resistivity (ρ) (see Sec. S3 of SM [30]) exhibits activated behavior [$\rho = \rho_0 \exp(E_a/K_B T)$, E_a is the activation energy] with $E_a \approx 80$ meV, which is very similar to the value observed in the bulk [11,31]. Further transport analysis strongly suggests that the antiferromagnetic transition temperature ($T_N \sim 120$ K) is very similar to the bulk PTO (see Sec. S3 of SM [30]). This is not surprising considering T_N showed very little change in high pressure experiment in case of bulk $LaTiO_3$ [32].

B. Synchrotron x-ray diffraction and x-ray linear dichroism

In order to probe the structural quality of the thin film, we performed the reciprocal space mapping and the crystal truncation rod measurements at the 33-ID beamline of the Advanced Photon Source, USA. The crystal truncation rods (CTRs) are measured using a six-circle diffractometer with x-ray energy of 15.5 keV ($\lambda = 0.7999$ Å). The different specular and off-specular CTRs are scanned along the vertical reciprocal space coordinate L (in the reciprocal lattice unit of pseudocubic NGO) with a maximum value of $L_{max} = 5.8$; for other reciprocal space coordinates, $H_{max} = K_{max} = 2$. The

two-dimensional image of the diffraction spot at each step of L is recorded with a pixel array area detector (Dectris PILATUS 100K). To extract the intensity, we have carefully removed the background and integrated over a small region around the diffraction spot for each image followed by a geometric factor correction of the spectra. XLD measurements were carried out at the beamline 4.0.2 of the Advanced Light Source, USA using total electron yield mode (probing depth at least 5 nm for Ti $L_{3,2}$ edges). To minimize surface oxidation, a 10 uc PTO film, capped by 2.5 nm amorphous AlO_x has been used for these synchrotron measurements.

C. First-principles density functional theory calculation

We performed first-principles density functional theory (DFT) [33] calculations using the VASP package [34] based on a plane-wave basis set and projector augmented wave method [35,36]. For the treatment of exchange correlation, Perdew-Burke-Ernzerhof generalized gradient approximation (GGA) [37] augmented by the Hubbard-U corrections (GGA+U) [38,39] has been considered. The Coulomb $U_{eff}(=U-J)$ values of 2.5 eV and 6 eV for Ti $3d$ and Pr $4f$ states, respectively, have been used [40]. The plane-wave energy cutoff was set to 520 eV. $9 \times 9 \times 7$ and $12 \times 12 \times 8$ meshes were used for Brillouin zone integrations in geometry optimization and electronic structure calculation, respectively. For the purpose of consideration of the $GdFeO_3$ -type distortion effect introduced by the substrate, we fixed lattice parameters to the experimentally observed values and relaxed only the internal atomic coordinates. The force convergence criterion was set to 0.001 eV/Å. To analyze the electronic properties in a more precise way, the band structure and DOS results are rotated from the global basis to the TiO_6 local basis. Further, we have performed wannierization on the DFT results using the WANNIER90 code [41] for the purpose of visualizing the most occupied natural orbitals for some bands, which are in a specific energy range.

III. RESULTS

A. Structural characterization of PTO thin film

Our reciprocal space mapping using synchrotron x-ray demonstrates that the PTO film is coherently strained with the underlying substrates [Figs. 1(a) and 1(b)]. The key ingredient behind the proposed mechanism of FOO in antiferromagnetic $RETiO_3$ is the presence of antiparallel displacement of RE sites due to $GdFeO_3$ -type distortion [17] (also see Sec. S1 of SM [30]). To determine the RE -site displacements and octahedral rotational pattern (ORP), half-order crystal truncation rods have been examined by synchrotron XRD. The presence of the $(0 \ 1/2 \ 2)_{pc}$ and the absence of the $(1/2 \ 0 \ 2)_{pc}$ Bragg peak for both NGO substrate and the PTO film [Fig. 1(c)] exclusively demonstrate the antiparallel displacement of RE sites within both film and substrate and confirm that the film has the same in-plane orientation as the NGO substrate and that the film is monodomain [42]. The ORP is represented by Glazer notation [43]. Diffraction measurements around certain half-order Bragg reflections [see Fig 1(d)] have found $a^-b^+c^-$ ORP for our PTO film, similar to the bulk PTO.

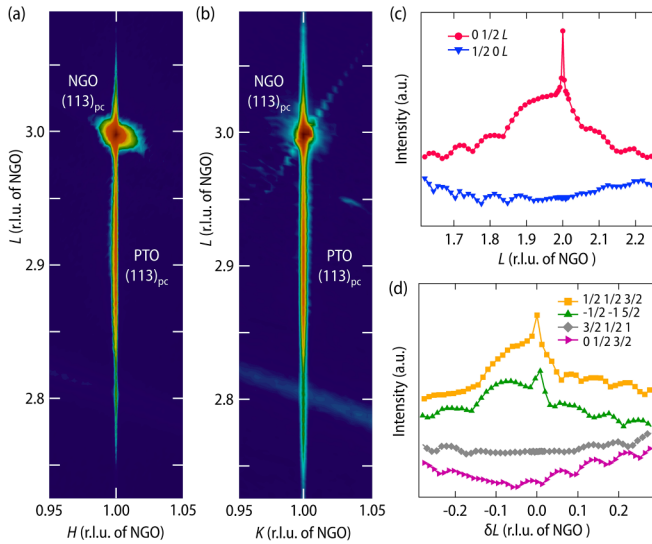


FIG. 1. (a) and (b) show the reciprocal space mappings onto the H - L and K - L plane, respectively. The intensity of the $(113)_{pc}$ diffraction spots, from both the substrate and the film, peak at same H [in (a)] and K [in (b)] values, signifying the coherently strained nature of the film. Thus, in-plane lattice constants of the film are $a_{IP} = 3.863 \text{ \AA}$, $b_{IP} = 3.854 \text{ \AA}$ [see Supplemental Material (SM) [30], Sec. S1]. Elongation of the out of plane lattice constant $c_{OP} \sim 4.011 \text{ \AA}$ compared to the bulk PTO arises due to the compressive strain from the substrate. (c) L scan around the $(0 \ 1/2 \ 2)_{pc}$ and $(1/2 \ 0 \ 2)_{pc}$ crystal truncation rods. (d) Octahedral rotational pattern has been determined by L scan centered around different half-order diffraction ($H' \ K' \ L'$) spots ($\delta L = L - L'$). The in-phase (+) rotation of the octahedra along the pseudocubic z axis produces $(H/2 \ K/2 \ L/2)_{pc}$ -type half-order reflections where L is an even integer and both H, K are odd integers with $H \neq K$ [43]. On the other hand, $(H/2 \ K/2 \ L/2)_{pc}$ -type reflections (with H, K, L are odd and $H \neq K$) appear from the antiphase (-) rotation [43]. Following these, the absence of the $(3/2 \ 1/2 \ 1)_{pc}$ peak signifies the absence of c^+ -type rotation. The observation of a $(-1/2 \ -1 \ 5/2)_{pc}$ peak confirms the b^+ pattern. The absence of the $(0 \ 1/2 \ 3/2)_{pc}$ reflection and observation of the $(1/2 \ 1/2 \ 3/2)_{pc}$ establishes the a^- rotation. We further observe that every film peak is associated with a NGO substrate peak.

B. Determination of the orbital symmetry

To directly probe the orbital structure, we have chosen XLD spectroscopy. In this technique, x-ray absorption spectra are recorded with linearly polarized x rays having the electric field vector parallel and perpendicular to the sample surface [27,44–49]. Due to the strong dependence of the absorption process on the angle between photon polarization vector and crystallographic axis, Ti $L_{3,2}$ ($2p \rightarrow 3d$) XAS for $E||xy$ (I_H) and $E||z$ (I_V) [see Fig. 2(a) for experimental geometry] probes the unoccupied in-plane (e.g., d_{xy} , $d_{x^2-y^2}$) and out-of-plane (e.g., d_{xz} , d_{yz} , $d_{3z^2-r^2}$) orbitals, respectively [49]. Thus, the sign of XLD ($= I_V - I_H$) can disclose even small energy splitting between sub-bands and their orbital characters [45–48,50], and XLD technique is used very often to probe orbital ordering [51–53]. We have measured XLD at 30 K and 300 K to probe the orbital state in the antiferromagnetic and paramagnetic phases, respectively [26,28,29,54].

The average Ti XAS [$(I_V + I_H)/2$], which probes the oxidation state, has been shown in Fig. 2(b). Comparing our

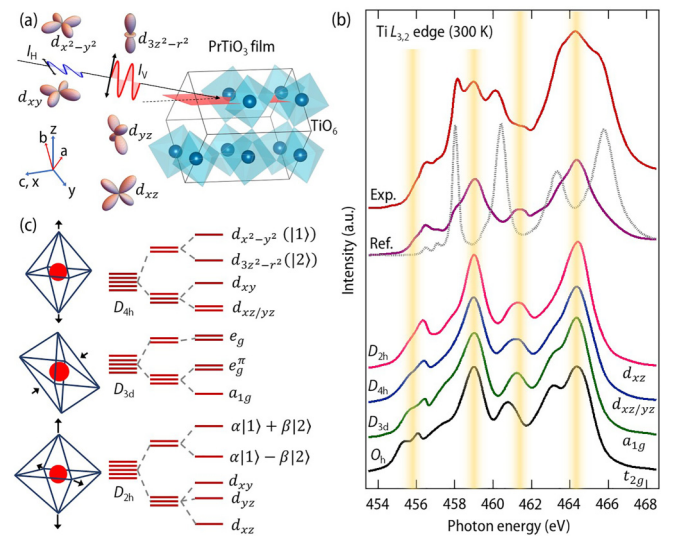


FIG. 2. (a) Schematic of the XLD experiment in grazing incidence geometry (with incident angle of 20° from the $(110)_{or}$ plane, shown in red). The crystallographic axes are denoted as a, b, c whereas the experiment and the simulations are performed in pseudocubic x, y, z coordinate. (b) Experimentally observed XAS data at Ti $L_{3,2}$ edge at 300 K (red). For comparison, the Ti^{3+} (purple) and Ti^{4+} (gray) reference spectra, normalized to equal integral spectral weight, are adapted from [8]. Considering the experimental configuration, Ti- $L_{3,2}$ XAS is simulated for orthorhombic (D_{2h}), tetragonal (D_{4h}), trigonal (D_{3d}), octahedral (O_h) symmetry. The corresponding resulting splitting of the d levels have been shown in (c).

experimental data at 300 K with the reference spectra for Ti^{3+} and Ti^{4+} [8], we observe XAS features of the desired Ti^{3+} together with unwanted Ti^{4+} in our PTO film. Such Ti^{4+} appears due to surface oxidation and is very common in $RETiO_3$ thin films [8,55]. Using these Ti^{3+} and Ti^{4+} reference XAS spectra with equal integrated spectral weight, we find that 75–80 % Ti are with +3 oxidation state (analysis shown in Sec. S5 of SM [30]). The absence of any impurity phase in the $(0 \ 0 \ L)_{pc}$ scan of XRD (see Sec. S4 of SM [30]) and the confirmation of bulk PTO-like electrical transport behavior and orthorhombic symmetry of the ultrathin PTO film strongly suggest that the excess interstitial oxygen atoms are distributed randomly in the film without affecting its electronic and structural behaviors. We have focused on analyzing XAS and XLD features related to the Ti^{3+} , which are highlighted by yellow shade around 455 eV, 459 eV, 461 eV, and 464 eV in Fig. 2(b).

The XAS line shape strongly depends on the local structural symmetry of the TiO_6 unit. Mochizuki and Imada considered the crystal field with D_{3d} symmetry under trigonal compression [17]. In the absence of any octahedral tilt and rotation, the wave function of the lowest occupied state (a_{1g} orbital) for D_{3d} symmetry [Fig. 2(c)] is $1/\sqrt{3}$ ($d_{xy} + d_{yz} + d_{xz}$). The low-temperature NMR spectra were explained assuming the existence of such orbitals [25]. However, different Ti-O bond lengths of a TiO_6 octahedron, obtained from diffraction experiments [28,56], do not follow the D_{3d} symmetry, and the symmetry should rather be D_{2h} [57]. Several theoretical studies also predicted that the occupied orbital of Ti has dominant ($d_{yz} + d_{xz}$) orbital character in the presence

of GdFeO₃-type distortions [18,20]. The presence of epitaxial strain in thin film samples will add further complexity to the problem. For example, in the present case, the compressive strain might induce a tetragonal distortion (D_{4h} symmetry with an in-plane compression). Therefore, we have considered four possible crystal fields: O_h , D_{3d} , D_{2h} , and D_{4h} [see Fig. 2(c)] and have simulated $L_{3,2}$ -edge XAS spectra of Ti^{3+} using ligand field multiplet theory-based QUANTY program [58]. The value of all parameters used in the simulations have been listed in Ref. [59].

The spectrum, especially the features within 454–456 eV, simulated with O_h symmetry does not agree with the observed Ti^{3+} spectra [26], indicating a lifting of degeneracy for the t_{2g} states [Fig. 2(b)]. We have also simulated the XAS considering the trigonal compression (D_{3d} symmetry with occupied a_{1g} state), as per the theoretical prediction [17] and for tetragonal elongation (D_{4h} symmetry with occupied d_{xz}/d_{yz} state), which is generally expected under a compressive strain. Our simulated spectra in both cases show a good agreement with the reference spectra [see Fig. 2(b)]. Finally, we consider the D_{2h} symmetry where the lowest occupied orbital has d_{xz} character. This simulated spectrum matches very well with the reference one. However, the simulated spectrum of D_{2h} symmetry with either d_{xy} or d_{yz} as the lowest orbital is very different (see Sec. S7 of SM [30]). We further note that a gap (Δ_{gap}) of 0.35–0.50 eV between the lowest occupied and the next unoccupied state was necessary for each D_{3d} , D_{4h} , and D_{2h} symmetry to match the spectra. These results demonstrate that while isotropic XAS can definitively conclude the existence of noncubic crystal field, it fails to determine the symmetry of the occupied orbital.

To find out the orbital state, we have focused on polarization-dependent absorption spectra and XLD [Figs. 3(a) and 3(b)] at the paramagnetic phase, where XLD is contributed by anisotropic charge distribution only [49]. In order to understand the origin of finite XLD feature, we have simulated XLD spectra for the three different noncubic crystal fields considering the experimental geometry [denoted by xyz coordinate system in Fig. 2(a)]. In the D_{4h} symmetry the line shape of the simulated XLD spectra is markedly different from the experimental data. In D_{3d} symmetry with a_{1g} as the lowest orbital, although the XLD features match around 455 eV and 461 eV, large deviations are observed around 459 eV and 464 eV. As evident, the spectra simulated in the D_{2h} symmetry with d_{xz} as the lowest orbital shows best agreement with our experimental observation. Moreover, simulated XLD of D_{2h} symmetry for alternative cases with d_{yz} and d_{xy} as the lowest state do not match with our experimental observation (see Sec. S7 of SM [30]). This establishes that the electron occupies predominantly d_{xz} orbital in D_{2h} symmetry. To further testify whether any arbitrary value of Δ_{gap} within D_{2h} symmetry can result orbital polarization, we have simulated a series of XLD spectra (shown in Sec. S9 of SM [30]) and find that spectra with $\Delta_{\text{gap}} \sim 300$ –500 meV only match with our experimental observation. This implies that the electron occupies a nondegenerate orbital, that is energetically well separated from remaining ones. This energetics should lock the orbitals spatially, resulting in a FOO rather than OL, in the paramagnetic phase. Such large orbital splitting results quenching of the orbital

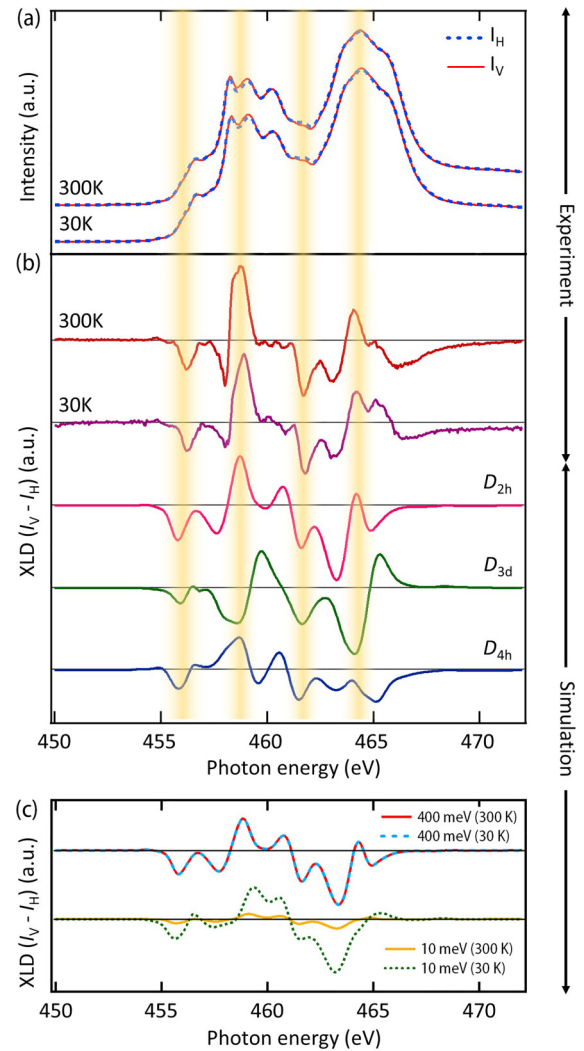


FIG. 3. (a) $\text{Ti } L_{3,2}$ edge XAS spectra recorded in two different polarizations (I_V and I_H) at 300 K and at 30 K. (b) shows the experimental XLD ($I_V - I_H$) data at 300 K and 30 K and simulated XLD data in experimental geometry for different symmetries of the TiO_6 octahedron. We also note that the sign of simulated XLD line shape remains unaffected in presence of the octahedral tilting (see Sec. S8 of SM [30]). (c) XLD spectra in D_{2h} symmetry is simulated for $\Delta_{\text{gap}} = 400$ meV (top) and 10 meV (bottom) at 300 K and 30 K.

moment [26], which would lead to temperature insensitivity of XAS and XLD line shape. Indeed, we observe the same in our experiments [Figs. 3(a) and 3(b)], further corroborated by temperature-dependent (30 K and 300 K) XLD simulation with large gap [Fig. 3(c), $\Delta_{\text{gap}} = 400$ meV]. However, the XLD spectra would become strongly temperature dependent when we considered a smaller gap (e.g., $\Delta_{\text{gap}} = 10$ meV) (also see Sec. S10 of SM [30]). Thus, we establish that in presence of large orthorhombic distortion, the same orbital ordering pattern is also preserved in the antiferromagnetic phase.

C. Results from DFT calculation

Our XLD experiments on thin film of PrTiO_3 , in conjunction with cluster calculation, have demonstrated the existence

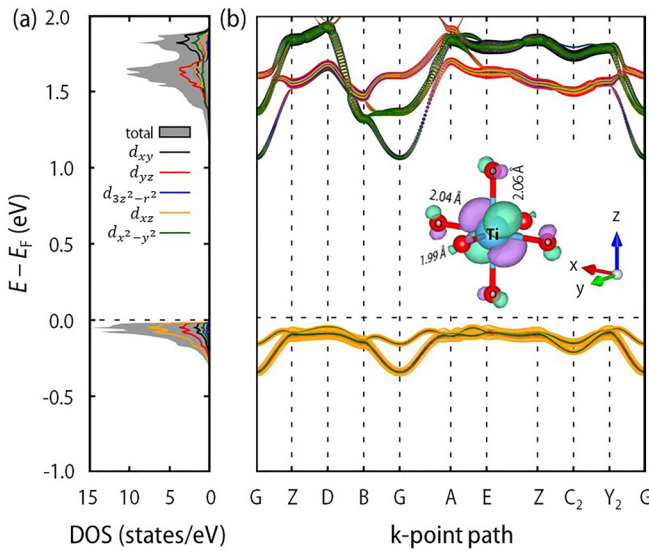


FIG. 4. (a) Calculated DOS and (b) electronic band structure for majority spin channel. lm -decomposed data are plotted in the TiO_6 local basis. Black, red, blue, yellow, and green curves (dots) represent d_{xy} , d_{yz} , $d_{3z^2-r^2}$, d_{xz} , $d_{x^2-y^2}$, respectively. Fermi level is set to zero. The inset of (b) shows the MLWFs obtained on each TiO_6 octahedron. The constant value surfaces with lobes of different signs are colored as purple and cyan.

of ferro-orbital ordering. To testify whether epitaxial strain plays any role in stabilizing this FOO phase, we performed first-principles studies for PrTiO_3 with (i) bulk lattice constants and (ii) our thin film lattice parameters. A TiO_6 octahedron from the relaxed structure for the second case is shown in the inset of Fig. 4. According to the bond length differences, the six Ti-O bonds around the center Ti atom can be classified into three categories, and hence, we defined the local basis of all the TiO_6 octahedra in the following way: z and y axes are along the directions with the longest and the shortest Ti-O bond length, respectively (2.06 and 1.99 Å) whereas the x axis is along the other direction (with the bond length equals to 2.04 Å), which give each octahedron a local D_{2h} symmetry. As shown in the electronic density of states [Fig. 4(a)] and band structure [Fig. 4(b)] plot, the occupied states of the Ti atom have mostly d_{xz}/d_{yz} orbitals with a dominant contribution from the d_{xz} orbitals while the $d_{3z^2-r^2}$ and $d_{x^2-y^2}$ orbitals are almost degenerate with a nearly zero occupation. The two bands just below the Fermi level are represented by the maximally localized Wannier functions (MLWFs). As it can be seen in the inset of Fig. 4(b), within the proper TiO_6 local basis, the most occupied natural orbitals have a perfect d_{xz} shape. Therefore, these results are in excellent agreement with the experimental finding of d_{xz} character of the occupied non-degenerate orbital. We have further plotted charge isosurfaces corresponding to the two occupied bands located just below the Fermi energy, which also demonstrates the existence of

FOO (see Sec. S11 of SM [30]). The calculation of bulk PTO yields very similar DOS features (shown in Sec. S12 of SM [30]), demonstrating that the observation of FOO is not linked to the underlying epitaxial strain. Additionally, our first-principle simulations show that varying magnetic states leads to minor modifications of the electronic structure, the d_{xz} character of the occupied orbital remains unaffected by such changes, further demonstrating the dominant contribution of the orthorhombic distortion (see Sec. S13 of SM [30]).

IV. CONCLUSIONS

To conclude, our present work conclusively demonstrates that the D_{2h} crystal field splitting of PrTiO_3 is strong enough to have a nondegenerate occupied orbital in both paramagnetic and antiferromagnetic phases, which is well separated ($\Delta_{\text{gap}} \approx 400$ meV) from the remaining orbital manifold. Most importantly, this energy gap is larger than the energy scales of the orbital fluctuations coupled to the lattice vibrations [60], superexchange interaction-driven spin-orbital resonance, estimated from orbital liquid model [15], as well as the thermal energy scale, leading to orbital ordering. Therefore, we conclusively demonstrate the existence of orbital ordered phase both in the paramagnetic and antiferromagnetic phases of PrTiO_3 , which is primarily contributed by the orthorhombic distortion, settling a longstanding debate about the spin-orbital physics of antiferromagnetic $RE\text{TiO}_3$.

ACKNOWLEDGMENTS

The authors acknowledge AFM, XRD, wire bonding facilities of the Department of Physics, IISc Bangalore. S.M. acknowledges DST Nanomission grant (DST/NM/NS/2018/246) and SERB Core Research grant (CRG/2022/001906) for financial support. This research used resources of the Advanced Photon Source, a U.S. Department of Energy Office of Science User Facility operated by Argonne National Laboratory under Contract No. DE-AC02-06CH11357. This research used resources of the Advanced Light Source, which is a Department of Energy Office of Science User Facility under Contract No. DE-AC02-05CH11231. The computations were enabled in project SNIC 2021/3-38 by resources provided to B.S. by the Swedish National Infrastructure for Computing (SNIC) at NSC, PDC and HPC2N partially funded by the Swedish Research Council through Grant Agreement No. 2018-05973. B.S. acknowledges allocation of supercomputing hours by PRACE DECI-17 project ‘Q2Dtopomat’ in Eagle supercomputer in Poland and EuroHPC resources in Karolina supercomputer in Czech Republic. B.S. and S.M. acknowledge Indo-Swedish Joint Network Grant No. 2018 provided by Swedish Research Council (Grant No. 2018-07082). B.S. also acknowledges financial support from Swedish Research Council (Grant No. 2022-04309).

- [1] J. S. Griffith, *The Theory of Transition-Metal Ions* (Cambridge University Press, Cambridge, 1964).
 [2] D. Khomskii, *ECS J. Solid State Sci. Technol.* **11**, 054004 (2022).

- [3] K. Kugel and D. Khomskii, *Zh. Eksp. Teor. Fiz.* **64**, 1429 (1973).
 [4] D. Khomskii, *Transition Metal Compounds* (Cambridge University Press, Cambridge, 2014).

- [5] Y. Tokura and N. Nagaosa, *Science* **288**, 462 (2000).
- [6] S. V. Streltsov and D. I. Khomskii, *Phys. Usp.* **60**, 1121 (2017).
- [7] M. Imada, A. Fujimori, and Y. Tokura, *Rev. Mod. Phys.* **70**, 1039 (1998).
- [8] P. Scheiderer, M. Schmitt, J. Gabel, M. Zapf, M. Stübinger, P. Schütz, L. Dudy, C. Schlueter, T.-L. Lee, M. Sing, and R. Claessen, *Adv. Mater.* **30**, 1706708 (2018).
- [9] J. Liu, K. Hejazi, and L. Balents, *Phys. Rev. Lett.* **121**, 107201 (2018).
- [10] S. Chaudhary, D. Hsieh, and G. Refael, *Phys. Rev. B* **100**, 220403(R) (2019).
- [11] H. D. Zhou and J. B. Goodenough, *J. Phys.: Condens. Matter* **17**, 7395 (2005).
- [12] H. Nakao, Y. Wakabayashi, T. Kiyama, Y. Murakami, M. v. Zimmermann, J. P. Hill, D. Gibbs, S. Ishihara, Y. Taguchi, and Y. Tokura, *Phys. Rev. B* **66**, 184419 (2002).
- [13] M. Mochizuki and M. Imada, *New J. Phys.* **6**, 154 (2004).
- [14] T. Mizokawa and A. Fujimori, *Phys. Rev. B* **54**, 5368 (1996).
- [15] G. Khaliullin and S. Maekawa, *Phys. Rev. Lett.* **85**, 3950 (2000).
- [16] M. Mochizuki and M. Imada, *J. Phys. Soc. Jpn.* **70**, 2872 (2001).
- [17] M. Mochizuki and M. Imada, *Phys. Rev. Lett.* **91**, 167203 (2003).
- [18] E. Pavarini, S. Biermann, A. Poteryaev, A. I. Lichtenstein, A. Georges, and O. K. Andersen, *Phys. Rev. Lett.* **92**, 176403 (2004).
- [19] E. Pavarini, A. Yamasaki, J. Nuss, and O. K. Andersen, *New J. Phys.* **7**, 188 (2005).
- [20] J. Varignon, M. N. Grisolia, D. Preziosi, P. Ghosez, and M. Bibes, *Phys. Rev. B* **96**, 235106 (2017).
- [21] D. A. MacLean, H.-N. Ng, and J. E. Greedan, *J. Solid State Chem.* **30**, 35 (1979).
- [22] G. I. Meijer, W. Henggeler, J. Brown, O.-S. Becker, J. G. Bednorz, C. Rossel, and P. Wachter, *Phys. Rev. B* **59**, 11832 (1999).
- [23] B. Keimer, D. Casa, A. Ivanov, J. W. Lynn, M. v. Zimmermann, J. P. Hill, D. Gibbs, Y. Taguchi, and Y. Tokura, *Phys. Rev. Lett.* **85**, 3946 (2000).
- [24] M. Cwik, T. Lorenz, J. Baier, R. Müller, G. André, F. Bourée, F. Lichtenberg, A. Freimuth, R. Schmitz, E. Müller-Hartmann, and M. Braden, *Phys. Rev. B* **68**, 060401(R) (2003).
- [25] T. Kiyama and M. Itoh, *Phys. Rev. Lett.* **91**, 167202 (2003).
- [26] M. W. Haverkort, Z. Hu, A. Tanaka, G. Ghiringhelli, H. Roth, M. Cwik, T. Lorenz, C. Schüßler-Langeheine, S. V. Streltsov, A. S. Mylnikova, V. I. Anisimov, C. de Nadai, N. B. Brookes, H. H. Hsieh, H.-J. Lin, C. T. Chen, T. Mizokawa, Y. Taguchi, Y. Tokura, D. I. Khomskii *et al.*, *Phys. Rev. Lett.* **94**, 056401 (2005).
- [27] J. Chakhalian, J. W. Freeland, H.-U. Habermeier, G. Cristiani, G. Khaliullin, M. van Veenendaal, and B. Keimer, *Science* **318**, 1114 (2007).
- [28] A. C. Komarek, H. Roth, M. Cwik, W.-D. Stein, J. Baier, M. Kriener, F. Bourée, T. Lorenz, and M. Braden, *Phys. Rev. B* **75**, 224402 (2007).
- [29] X.-J. Zhang, E. Koch, and E. Pavarini, *Phys. Rev. B* **102**, 035113 (2020).
- [30] See Supplemental Material at <http://link.aps.org/supplemental/10.1103/PhysRevB.108.045145> for pseudocubic notation, thin film growth and characterization, dc electrical transport measurement, synchrotron XRD and fitting, estimation of $\text{Ti}^{3+}/\text{Ti}^{4+}$ form XAS, Ti 3d level splitting in different symmetries of crystal field, XAS and XLD simulation in D_{2h} symmetry for different occupied orbitals, effect of octahedral tilting on XLD, determination of the strength of orthorhombic distortion, dependence of thermal occupation on orthorhombic distortion, FOO from DFT calculation, effect of strain on orbital ordering and orbital occupation in different magnetic configuration, which include Ref. [61–77].
- [31] T. Katsufuji, Y. Taguchi, and Y. Tokura, *Phys. Rev. B* **56**, 10145 (1997).
- [32] Y. Okada, T. Arima, Y. Tokura, C. Murayama, and N. Môri, *Phys. Rev. B* **48**, 9677 (1993).
- [33] W. Kohn and L. J. Sham, *Phys. Rev.* **140**, A1133 (1965).
- [34] G. Kresse and J. Furthmüller, *Comput. Mater. Sci.* **6**, 15 (1996).
- [35] P. E. Blöchl, *Phys. Rev. B* **50**, 17953 (1994).
- [36] G. Kresse and D. Joubert, *Phys. Rev. B* **59**, 1758 (1999).
- [37] J. P. Perdew, K. Burke, and M. Ernzerhof, *Phys. Rev. Lett.* **77**, 3865 (1996).
- [38] V. I. Anisimov, F. Aryasetiawan, and A. I. Lichtenstein, *J. Phys.: Condens. Matter* **9**, 767 (1997).
- [39] S. L. Dudarev, G. A. Botton, S. Y. Savrasov, C. J. Humphreys, and A. P. Sutton, *Phys. Rev. B* **57**, 1505 (1998).
- [40] J. Betancourt, T. R. Paudel, E. Y. Tsymlal, and J. P. Velev, *Phys. Rev. B* **96**, 045113 (2017).
- [41] G. Pizzi, V. Vitale, R. Arita, S. Blügel, F. Freimuth, G. Géranton, M. Gibertini, D. Gresch, C. Johnson, T. Koretsune *et al.*, *J. Phys.: Condens. Matter* **32**, 165902 (2020).
- [42] S. Middey, D. Meyers, R. Kumar Patel, X. Liu, M. Kareev, P. Shafer, J.-W. Kim, P. Ryan, and J. Chakhalian, *Appl. Phys. Lett.* **113**, 081602 (2018).
- [43] A. M. Glazer, *Acta Cryst. A* **31**, 756 (1975).
- [44] D. Pesquera, G. Herranz, A. Barla, E. Pellegrin, F. Bondino, E. Magnano, F. Sánchez, and J. Fontcuberta, *Nat. Commun.* **3**, 1189 (2012).
- [45] M. Salluzzo, J. C. Cezar, N. B. Brookes, V. Bisogni, G. M. De Luca, C. Richter, S. Thiel, J. Mannhart, M. Huijben, A. Brinkman *et al.*, *Phys. Rev. Lett.* **102**, 166804 (2009).
- [46] M. Salluzzo, S. Gariglio, D. Stornaiuolo, V. Sessi, S. Rusponi, C. Piamonteze, G. M. De Luca, M. Minola, D. Marré, A. Gadaleta *et al.*, *Phys. Rev. Lett.* **111**, 087204 (2013).
- [47] Y. Cao, X. Liu, P. Shafer, S. Middey, D. Meyers, M. Kareev, Z. Zhong, J.-W. Kim, P. J. Ryan, E. Arenholz *et al.*, *npj Quantum Mater.* **1**, 16009 (2016).
- [48] J.-S. Lee, Y. W. Xie, H. K. Sato, C. Bell, Y. Hikita, H. Y. Hwang, and C.-C. Kao, *Nat. Mater.* **12**, 703 (2013).
- [49] J. Stöhr and H. C. Siegmann, *Solid-State Sciences* (Springer, Berlin, 2006).
- [50] P. Mandal, R. K. Patel, D. Rout, R. Banerjee, R. Bag, K. Karmakar, A. Narayan, J. W. Freeland, S. Singh, and S. Middey, *Phys. Rev. B* **103**, L060504 (2021).
- [51] D. J. Huang, W. B. Wu, G. Y. Guo, H.-J. Lin, T. Y. Hou, C. F. Chang, C. T. Chen, A. Fujimori, T. Kimura, H. B. Huang, A. Tanaka, and T. Jo, *Phys. Rev. Lett.* **92**, 087202 (2004).
- [52] F. Iga, M. Tsubota, M. Sawada, H. B. Huang, S. Kura, M. Takemura, K. Yaji, M. Nagira, A. Kimura, T. Jo, T. Takabatake, H. Namatame, and M. Taniguchi, *Phys. Rev. Lett.* **93**, 257207 (2004).
- [53] J. M. Chen, Z. Hu, H. T. Jeng, Y. Y. Chin, J. M. Lee, S. W. Huang, K. T. Lu, C. K. Chen, S. C. Haw, T. L. Chou, H.-J. Lin, C. C. Shen, R. S. Liu, A. Tanaka, L. H. Tjeng, and C. T. Chen, *Phys. Rev. B* **81**, 201102(R) (2010).

- [54] J.-G. Cheng, Y. Sui, J.-S. Zhou, J. B. Goodenough, and W. H. Su, *Phys. Rev. Lett.* **101**, 087205 (2008).
- [55] R. Aeschlimann, D. Preziosi, P. Scheiderer, M. Sing, S. Valencia, J. Santamaria, C. Luo, H. Ryll, F. Radu, R. Claessen *et al.*, *Adv. Mater.* **30**, 1707489 (2018).
- [56] M. Eitel and J. Greedan, *J. Less-Common Met.* **116**, 95 (1986).
- [57] I. V. Solov'yev, *Phys. Rev. B* **69**, 134403 (2004).
- [58] M. W. Haverkort, M. Zwierzycki, and O. K. Andersen, *Phys. Rev. B* **85**, 165113 (2012).
- [59] The parameters used in the calculation are listed as follows. Crystal field parameters: $D_q^{O_h} = 0.16$; $D_q^{D_{2h}} = 0.16$, $D_s^{D_{2h}} = 0.1$, $D_t^{D_{2h}} = 0.0$, $D_u^{D_{2h}} = -0.2$, $D_v^{D_{2h}} = 0.1$; $D_q^{D_{4h}} = 0.16$, $D_s^{D_{4h}} = 0.2$, $D_t^{D_{4h}} = 0.02$; $D_q^{D_{3d}} = 0.105$, $D_\sigma^{D_{3d}} = 0$, $D_r^{D_{3d}} = 0.05$. Charge transfer parameters: $\Delta = 4$, $U_{dd} = 4$, $U_{pd} = 6$. Hopping parameters: $V_{t_{2g}}^{O_h} = 2.5$, $V_{e_g}^{O_h} = 4$; $V_{a_g^2-y^2}^{D_{2h}} = 4$, $V_{a_g^2-y^2}^{D_{2h}} = 4$, $V_{b_{1g}}^{D_{2h}} = 2.5$, $V_{b_{2g}}^{D_{2h}} = 2.5$, $V_{b_{3g}}^{D_{2h}} = 2.5$, $V_{M_{4g}}^{D_{2h}} = 0.1$; $V_{a_{1g}}^{D_{4h}} = 4$, $V_{b_{1g}}^{D_{4h}} = 4$, $V_{b_{2g}}^{D_{4h}} = 2.5$, $V_{e_g}^{D_{4h}} = 2.5$; $V_{a_{1g}}^{D_{3d}} = 2.5$, $V_{e_g}^{D_{3d}} = 2.5$, $V_{e_g}^{D_{3d}} = 4.0$, $V_{M_{4g}}^{D_{3d}} = 0.1$. The value of all the parameters are in eV. The details of the parameters in different symmetry of the crystal field can be found at www.quanty.org (also see Sec. S6 of SM [30]). In the calculation, the strength of the spin-orbit splitting in the Ti 3d states is ≈ 20 meV, which is an order of magnitude smaller than Δ_{ECF} , similar to bulk LaTiO₃.
- [60] M. Reedyk, D. A. Crandles, M. Cardona, J. D. Garrett, and J. E. Greedan, *Phys. Rev. B* **55**, 1442 (1997).
- [61] L. Vasylechko, L. Akselrud, W. Morgenroth, U. Bismayer, A. Matkovskii, and D. Savytskii, *J. Alloys Compd.* **297**, 46 (2000).
- [62] P. Mandal, S. K. Ojha, R. K. Patel, S. Kumar, and S. Middey, *J. Phys. Chem. C* **125**, 12968 (2021).
- [63] M. Björck and G. Andersson, *J. Appl. Crystallogr.* **40**, 1174 (2007).
- [64] J. Hemberger, H.-A. Krug von Nidda, V. Fritsch, J. Deisenhofer, S. Lobina, T. Rudolf, P. Lunkenheimer, F. Lichtenberg, A. Loidl, D. Bruns, and B. Büchner, *Phys. Rev. Lett.* **91**, 066403 (2003).
- [65] I. Loa, X. Wang, K. Syassen, H. Roth, T. Lorenz, M. Hanfland, and Y. Mathis, *J. Phys.: Condens. Matter* **19**, 406223 (2007).
- [66] Q. Gan, R. Rao, C. Eom, J. Garrett, and M. Lee, *Appl. Phys. Lett.* **72**, 978 (1998).
- [67] H. Z. Guo, J. Burgess, E. Ada, S. Street, A. Gupta, M. N. Iliev, A. J. Kellock, C. Magen, M. Varela, and S. J. Pennycook, *Phys. Rev. B* **77**, 174423 (2008).
- [68] T. Fister, H. Zhou, Z. Luo, S. S. A. Seo, S. Hruszkewycz, D. Proffit, J. Eastman, P. Fuoss, P. Baldo, H. N. Lee *et al.*, *APL Mater.* **2**, 021102 (2014).
- [69] H. Zhou, Y. Yacoby, V. Y. Butko, G. Logvenov, I. Božović, and R. Pindak, *Proc. Natl. Acad. Sci. USA* **107**, 8103 (2010).
- [70] D. P. Kumah, S. Shusterman, Y. Paltiel, Y. Yacoby, and R. Clarke, *Nat. Nanotechnol.* **4**, 835 (2009).
- [71] P. R. Willmott, S. A. Pauli, R. Heger, C. M. Schlepütz, D. Martoccia, B. D. Patterson, B. Delley, R. Clarke, D. Kumah, C. Cionca, and Y. Yacoby, *Phys. Rev. Lett.* **99**, 155502 (2007).
- [72] A. S. Disa, D. P. Kumah, A. Malashevich, H. Chen, D. A. Arena, E. D. Specht, S. Ismail-Beigi, F. J. Walker, and C. H. Ahn, *Phys. Rev. Lett.* **114**, 026801 (2015).
- [73] R. Aeschlimann, M. N. Grisolia, G. Sanchez-Santolino, J. Varignon, F. Choueikani, R. Mattana, V. Garcia, S. Fusil, T. Fröhlich, M. Braden, B. Delley, M. Varela, P. Ohresser, J. Santamaria, A. Barthélémy, C. Piamonteze, and M. Bibes, *Phys. Rev. Mater.* **5**, 014407 (2021).
- [74] P. Xu, Y. Ayino, C. Cheng, V. S. Pribiag, R. B. Comes, P. V. Sushko, S. A. Chambers, and B. Jalan, *Phys. Rev. Lett.* **117**, 106803 (2016).
- [75] Y. Cao, P. Shafer, X. Liu, D. Meyers, M. Kareev, S. Middey, J. W. Freeland, E. Arenholz, and J. Chakhalian, *Appl. Phys. Lett.* **107**, 112401 (2015).
- [76] M. Haverkort, Ph.D. thesis, Universität zu Köln, 2005.
- [77] Y. Yuan, Y. Lu, G. Stone, K. Wang, C. M. Brooks, D. G. Schlom, S. B. Sinnott, H. Zhou, and V. Gopalan, *Nat. Commun.* **9**, 5220 (2018).